Model for Heat and Moisture Transfer in Arbitrarily Shaped Two-dimensional Porous Media

M. E. Casada, J. H. Young

Abstract. *A model was developed to predict heat and moisture transfer due to natural convection and diffusion in arbitrarily shaped two-dimensional porous media. Boundary conditions were diurnally varying ambient temperature on the outside of walls with moderate Biot number. Other important boundary conditions were developed for typical storage and transportation situations. A two-energy equation model was used to allow for the difference between the fluid and solid temperatures and its effect on mass transfer in the porous medium. The governing equations were solved with a finite-difference method in a generalized coordinate system using a stream function formulation. It was found that the energy and moisture transport equations were best solved using a modified Crank-Nicolson method that was developed to control the tendency for instability caused by the source terms in these equations. All of the boundary conditions that were developed worked satisfactorily The two-energy equation model predicted small differences between the fluid and solid particle temperatures and natural convection only impacted the temperature solution significantly in the upper comers of the porous media.* **Keywords.** *Grain storage, Numerical modeling, Transportation, Peanuts, Moisture.*

The temperature and moisture content of grain and similar hygroscopic biological products are generally considered to be the most important factors in controlling quality during storage (Ross et al., 1973; Muir, 1973; Smith and Davidson, 1982). Long-term (at least several weeks) moisture migration from natural convection currents induced by temperature gradients in stored grain is one well-known problem resulting from adverse temperatures during storage (Ross et al., 1973; Muir, 1973; Loewer et al., 1979; Pierce and Shelton, 1984; Wilcke and Fossen, 1986; Halderson et al., 1991; Khankari et al., 1993b). Safe relative humidity levels required to minimize deterioration during storage of biological products such as grains, seeds, and nuts are generally known and adhered to by producers and processors of these products. However, moisture migration during storage and transportation of these products may lead to localized areas with unsafe moisture levels causing unacceptable amounts of deterioration, even though the average moisture level in the lot is considered safe. Short-term (daily) moisture migration effects are also a potential problem because of the diurnally varying ambient conditions during storage and transportation.

Article was submitted for publication in December 1993; reviewed and approved for publication by the Food and Process Engineering Inst. of ASAE in June 1994. Presented as ASAE Paper No. 87-6512.

Approved as Paper No. 93306 of the Idaho Agricultural Experiment Station. Paper No. BAE 94-05 of the Journal Series of the Dept. of Biological and Agricultural Engineering, North Carolina State University, Raleigh. The use of trade names in this publication does not imply endorsement by the Idaho Agricultural Experiment Station or North Carolina Agricultural Research Service, of the products named, nor criticism of similar ones not mentioned.

The authors are **Mark E. Casada**, *ASAE Member Engineer*, Assistant Professor, Dept. of Agricultural Engineering, University of Idaho, Moscow; and **James H. Young**, *ASAE Fellow Engineer*, Professor, Dept. of Biological and Agricultural Engineering, North Carolina State University, Raleigh.

In this article, long-term moisture migration will be distinguished as that due to the natural convection currents. Short-term moisture migration is that due to the daily heating and cooling of the hygroscopic product. The heating for a few hours each day drives moisture from the product in the short-term. This moisture may also accumulate over a long time period, but these titles provide a convenient distinction between these two different phenomena.

Wooding (1957) and Combarnous and Bories (1975) gave the governing equations for natural convection in homogeneous porous media with Darcy flow (neglecting inertia):

Conservation of Mass (Air)

$$\phi \frac{\partial \rho}{\partial t} + \nabla \cdot \left(\rho \vec{V}\right) = 0 \tag{1}$$

Conservation of Momentum

$$\frac{\rho}{\phi} \frac{\partial \vec{V}}{\partial t} = -\nabla P + \rho \vec{g} - \frac{\mu}{K} \vec{V} \tag{2}$$

Conservation of Energy

$$\nabla \cdot \left(\bar{k}_f \nabla T_f\right) - \nabla \cdot \left[(\rho c)_f \vec{V} T_f\right] =$$

$$\frac{\partial}{\partial t}\left[\phi\,(\rho c)_f T_f\right] + h_p A_{s/v}\left(T_f - T_s\right) \tag{3}$$

$$\nabla \cdot \left(\bar{k}_s \nabla T_s\right) =$$

$$\frac{\partial}{\partial t}\left[(1-\phi)(\rho c)_s T_s\right] + h_p A_{s/v}\left(T_s - T_f\right) \tag{4}$$

  0001-2351 / 94 / 3706-1927

FLUID EQUATION OF STATE

$$\rho = \rho_o [\, 1 - \alpha_e (T_f - T_o) \,] \qquad (5)$$

The Darcy flow (Darcy, 1856; Bear, 1972) used by those authors was based on the assumption that the velocity was linearly related to the hydraulic gradient and required a value of less than one for the particle Reynolds number, Re_p. Equations 3 and 4 together enforce conservation of thermal energy when a temperature difference between the solid and fluid is included in the model. Combarnous and Bories (1975) pointed out that it might be difficult to determine some of the parameters in these equations: the equivalent thermal conductivity tensors, $\bar{k}_f$ and $\bar{k}_s$, and the heat transfer coefficient, h_p. Some results reported in the literature can be used to find h_p (Wakao and Kaguei, 1982), but $\bar{k}_f$ and $\bar{k}_s$ still present a problem. Combarnous and Bories (1975) studied the effect of h and constant values $\bar{k}_f$ and $\bar{k}_s$ on the numerical predictions of heat transfer in a rectangular enclosure using the stream function formulation. They found generally good agreement with experimental results (Combarnous and Bories, 1974) when they varied the values of $\bar{k}_f$ and $\bar{k}_s$ and h_p to fit their data.

There have been several numerical studies on natural convection heat transfer in porous media for recirculating flows in enclosures. The majority of these studies were based on the assumption of Darcy flow. Prasad and Kulacki (1984a, b) presented a stream function formulation from Wooding's (1957) equations for the natural convection problem in a rectangular porous medium assuming Darcy flow. This method has been used to solve a variety of problems in rectangular enclosures with different boundary conditions (Prasad, 1987; Prasad and Kulacki, 1986, 1987; El-Khatib and Prasad, 1987). The stream function formulation was used again by Stewart and Dona (1988) to predict the transient natural convection currents in grain storage bins. They used the modified Ergun equation from Patterson et al. (1971) to model the flow and they also found that the inertia term was only significant for particle Reynolds numbers greater than one. Vafai and Tein (1981) analytically developed a set of equations similar to those developed by Wooding (1957) using the local volume averaging technique. Unfortunately, that work did not overcome any difficulties in using such equation sets for solving heat transfer problems in porous media. The work mentioned above gives helpful guidelines for numerical solutions of heat transfer in porous media, but none of the researchers addressed the moisture transfer problem.

During the last 20 years, a number of models have been developed for heat transfer in stored grain in cylindrical bins, neglecting the interaction with moisture transfer (e.g., Jayas et al., 1992; who also listed most of the earlier works). Recently, a few models have been developed that include moisture transfer for stored grain in cylindrical bins (Tanka and Yoshida, 1984; Nguyen, 1986; Khankari et al., 1990; Obaldo et al., 1991; Abbouda et al., 1992; Khankari et al., 1993a, b). Singh et al. (1993) presented a three-dimensional finite difference model for stored grain in a rectangular enclosure. This model included estimates of dry matter loss and pesticide concentration, but used only simplified boundary conditions. None of these models were applicable to the irregular two-dimensional shape of railcars. Nor did these models address all of the boundary interactions that need to be studied in the railcar (e.g., air and moisture exchange with the headspace and the resulting solar heating interaction, variable resistance to heat transfer at the boundary due to variable air velocity and container walls, and temperature difference between the grain and air).

In order to use a given finite-difference solution with any possible arbitrary geometry to be specified, a body-fitted coordinate system is needed. The differential equation method is one of the most highly developed methods of generating body fitted coordinate systems (Anderson et al., 1984). This method transforms the arbitrarily shaped physical plane to a rectangular grid in the computational plane using differential equations to control the mapping. Thompson et al. (1974, 1977) gave a thorough presentation of using Poisson equations for each coordinate to perform these mappings. This method allowed for more control over the mesh spacing by the proper specifications of the source terms in the Poisson equations. Thompson (1978) provided information on using exponential functions for these source terms. The specification of boundary conditions for a few heat transfer and fluid flow cases in the computational plane was developed by Thames et al. (1975). They presented a method of enforcing a no-slip boundary condition on the vorticity transport equation that they found to work better than the methods of Israeli (1970) and Roache (1972). Peyret and Taylor (1983) presented the use of the finite-volume method for specifying the more complicated energy and moisture transfer boundary conditions. Thompson et al. (1977) and Thompson (1978) gave derivatives and vectors in the transformed plane that are needed for the finite-volume method. A few other needed relationships are given in Appendix A.

The need to determine the causes of moisture migration in shelled peanuts during transportation in railcars requires a model to predict moisture migration in the irregular shaped railcars. This is the first of two articles describing the development and application of such a model. This article describes the development of a numerical model with relevant boundary conditions for heat and moisture transfer in an arbitrarily shaped porous media, such as the peanut bed. The second article (Casada and Young, 1994) describes the application of this model to the transportation of peanuts and compares the model's predictions to experimental data.

The objective of this study was to develop a model for use on a personal computer for heat and moisture transfer in arbitrarily shaped two-dimensional porous media with the needed attributes included for studying both long-term and short-term moisture migration during transportation of peanuts. The major model attributes needed to study both types of moisture migration were: (1) accounting for the difference between the particle (peanut) and the fluid (air) temperature within the porous medium, (2) diurnally varying ambient temperature with variable finite resistance to heat transfer on the container surfaces, (3) air exchange allowed through the top surface of the porous medium, and (4) accounting for moisture movement due to temperature gradients, moisture gradients, and natural convection air currents.

GOVERNING EQUATIONS

Equation 2, conservation of momentum, was modified using Ergun's equation (Ergun, 1952) to include the effects of inertia equations 1 through 5 incorporate the assumptions of a homogeneous, isotropic porous medium and a fluid whose density varies linearly with temperature. Further assumptions are (Combarnous and Bories, 1975): (1) the changes in air density are much smaller than the densities themselves, so that the density variation is kept only in the buoyancy term, $\rho\vec{g}$, and (2) the thermal properties are constant.

A dimensionless stream function was defined by:

$$u = \phi \cdot \alpha_f \frac{\partial \psi}{\partial y} \tag{6a}$$

and

$$v = -\phi \cdot \alpha_f \frac{\partial \psi}{\partial x} \tag{6b}$$

The inertia terms were needed in the flow equations to properly describe flow reversals resulting from cycling boundary conditions.

Using Ergun's equation (Ergun, 1952),

$$\Delta P = F_1 \vec{V} + F_2 \left(\vec{V} \cdot \vec{V}\right) \vec{J} \tag{7}$$

adding a latent heat term in the solid energy equation, and adding an equation for transport of moisture in the pore spaces, the dimensionless governing equations in two dimensions become [see Prasad and Kulacki (1984a, b) for the basic stream function formulation of the continuity and momentum equations, and Casada (1990) for the modified formulation using equation 7, which includes the inertia term]:

$$F_v \frac{\partial^2 \psi}{\partial \bar{x}^2} + F_u \frac{\partial^2 \psi}{\partial \bar{y}^2} = Ra^* \frac{\partial \theta_f}{\partial \bar{x}} \tag{8}$$

$$\frac{\partial \theta_f}{\partial \bar{t}} + \psi_{\bar{x}} \frac{\partial \theta_f}{\partial \bar{y}} - \psi_{\bar{y}} \frac{\partial \theta_f}{\partial \bar{x}} + St_f \left(\theta_f - \theta_s\right) = \frac{1}{\phi}\left(\frac{\partial^2 \theta_f}{\partial \bar{x}^2} + \frac{\partial^2 \theta_f}{\partial \bar{y}^2}\right) \tag{9}$$

$$\frac{\partial \theta_s}{\partial \bar{t}} + St_s \left(\theta_s - \theta_f\right) = \frac{\alpha_s}{\alpha_f (1-\phi)}\left(\frac{\partial^2 \theta_s}{\partial \bar{x}^2} + \frac{\partial^2 \theta_s}{\partial \bar{y}^2}\right) + H_{fg} \frac{\partial \Omega}{\partial \bar{t}} \tag{10}$$

and

$$\frac{\partial \Gamma}{\partial \bar{t}} + \psi_{\bar{x}} \frac{\partial \Gamma}{\partial \bar{y}} - \psi_{\bar{y}} \frac{\partial \Gamma}{\partial \bar{x}} + St_m \left(\Gamma - \Gamma_s\right) = \frac{Le_f}{\phi}\left(\frac{\partial^2 \Gamma}{\partial \bar{x}^2} + \frac{\partial^2 \Gamma}{\partial \bar{y}^2}\right) \tag{11}$$

The thin-layer drying equation for hygroscopic particles such as grains and nuts, based on the exponential drying equation (Sherwood, 1936) is:

$$\Omega^{n+1} = \Omega^n + \frac{\phi St_m}{1-\phi} \frac{\rho_a}{\rho_s} \frac{\gamma_o}{M_o} \left(\Gamma_s - \Gamma\right) \Delta \bar{t} \tag{12}$$

This thin-layer model was used for convenience since the very low air to solid ratio results in the model not being sensitive to which thin-layer model was used.

The convective mass transfer coefficient, h_m, was calculated from the convective heat transfer coefficient for flow over a sphere using the Lewis analogy (Kays and Crawford, 1980) based on the actual interstitial air velocities. The equilibrium moisture content of the peanuts was calculated from the modified Henderson equation (ASAE, 1991). The values of $\bar{k}_f$ and $\bar{k}_s$, were estimated from the bulk thermal conductivity of peanuts based on the information in Combarnous and Bories (1974) and Masamune and Smith (1963). No explicit method of determining $\bar{k}_f$ and $\bar{k}_s$ is currently available. Peanut properties used were: $\bar{k}_f = 0.024$ W/mK, $\bar{k}_s = 0.085$ W/mK, $\rho_b = 652$ kg/m^3, $c_p = 2135$ J/kg K, and $K = 3.4 \times 10^{-8}$m^2. Air properties were taken from standard tables (Touloukian et al., 1970a, b, c).

In a generalized coordinate system where,

$$\xi = \xi(\bar{x}, \bar{y}) \tag{13a}$$

$$\eta = \eta(\bar{x}, \bar{y}) \text{ and} \tag{13b}$$

$$\tau = \bar{t} \tag{13c}$$

Equations 8, 9, 10, and 11 become (using the chain rule of calculus):

$$\alpha \frac{\partial^2 \psi}{\partial \xi^2} - 2\beta \frac{\partial^2 \psi}{\partial \eta \, \partial \xi} + \gamma \frac{\partial^2 \psi}{\partial \eta^2} + \delta \frac{\partial \psi}{\partial x} + \varepsilon \frac{\partial \psi}{\partial x} = Ra^* J \left(y_\eta \frac{\partial \theta_f}{\partial \xi} + y_\xi \frac{\partial \theta_f}{\partial \eta}\right) \tag{14}$$

$$\phi J^2 \left[\left(\frac{\partial \theta_f}{\partial \tau} - \frac{\psi_\eta}{J} \frac{\partial \theta_f}{\partial \xi} + \frac{\psi_\xi}{J} \frac{\partial \theta_f}{\partial \eta}\right) + St_f \left(\theta_f - \theta_s\right)\right] = \alpha \frac{\partial^2 \theta_f}{\partial \xi^2} - 2\beta \frac{\partial^2 \theta_f}{\partial \eta \, \partial \xi} + \gamma \frac{\partial^2 \theta_f}{\partial \eta^2} + \delta \frac{\partial \theta_f}{\partial \xi} + \varepsilon \frac{\partial \theta_f}{\partial \eta} \tag{15}$$

$$J^2 \left[\left(\frac{\partial \theta_s}{\partial \tau}\right) + St_s \left(\theta_s - \theta_f\right)\right] = \frac{\alpha_s}{\alpha_f (1-\phi)} \left(\alpha \frac{\partial^2 \theta_s}{\partial \xi^2} - 2\beta \frac{\partial^2 \theta_s}{\partial \eta \, \partial \xi} + \gamma \frac{\partial^2 \theta_s}{\partial \eta^2} + \delta \frac{\partial \theta_s}{\partial \xi} + \varepsilon \frac{\partial \theta_s}{\partial \eta}\right) + J^2 H_{fg} \frac{\partial \Omega}{\partial \tau} \tag{16}$$

and

$$\phi J^2\left[\left(\frac{\partial \Gamma}{\partial \tau}-\frac{\psi_\eta}{J}\frac{\partial \Gamma}{\partial \xi}+\frac{\psi_\xi}{J}\frac{\partial \Gamma}{\partial \eta}\right)+St_m(\Gamma-\Gamma_s)\right]=$$

$$Le_f\left(\alpha\frac{\partial^2\Gamma}{\partial\xi^2}-2\beta\frac{\partial^2\Gamma}{\partial\eta\,\partial\xi}+\gamma\frac{\partial^2\Gamma}{\partial\eta^2}+\delta\frac{\partial\Gamma}{\partial\xi}+\varepsilon\frac{\partial\Gamma}{\partial\eta}\right) \quad (17)$$

Equation 12 remains unchanged in the generalized coordinate system. Equations 14 through 17 may be solved in a computational plane, with a square mesh for simplified application of finite differences, while the results apply to the physical (real) plane because the geometry differences are accounted for by the metrics (x_ξ, x_η . . .) in these equations. The metrics may be calculated numerically after determining the x,y coordinates of the interior nodes from a numerical solution of the following equations (Thompson et al., 1977), which constitute the differential equation method of generating the computational grid:

$$\xi_{xx}+\xi_{yy}=P\ (\xi,\eta) \quad (18)$$

and

$$\eta_{xx}+\eta_{yy}=Q\ (\xi,\eta) \quad (19)$$

with the boundary conditions being the x,y coordinates of the boundary nodes in the physical plane. The source terms, P and Q, were specified to concentrate nodes near the boundaries where the gradients were larger, as discussed in Thompson et al. (1977).

Boundary Conditions

The following standard boundary conditions required for implementation of the finite-difference model were applied to the governing equations, equations 14 through 17, for use with the standard test simulation. These particular boundary conditions were chosen both because of their general applicability to storage and shipping containers and because they fit the primary intended application to shelled peanuts in railcars. Other useful alternative boundary conditions may be substituted as necessary with minimum impact on the rest of the model, as noted below. All boundary conditions discussed below were developed for the model. Those referred to as "standard" were used with the standard test simulation. Those referred to as "alternative" are available for applying the model to other situations. The boundary conditions are summarized in table 1 and the boundary domains are illustrated in figure 1.

Stream Function Equation

The standard boundary conditions on the stream function, equation 14, were constant stream function (ψ = zero) on all boundaries, including the line of symmetry. An important alternative boundary condition for the top boundary, which allows flow across the boundary was the condition,

Table 1. Boundary conditions used in the standard test simulation and alternative boundary conditions

	Eq. (No.)	Standard Boundary Condition	Alternative Boundary Conditions
Stream function	14	• $\psi = 0$ on all boundaries	• $\psi = 0$ on B_1, B_2, and B_3 • Eq. 20 on B_4
Fluid energy	15	• Conduction through wall with moderate Bi on B_1, B_2, B_4 Symmetry on B_3	• T = constant on all boundaries • Moderate Bi on B_4 • Wall conduction on B_3
Solid energy	16	• Conduction through wall with moderate Bi on B_1, B_2, B_4 Symmetry on B_3	• T = constant on all boundaries • Moderate Bi on B_4 • Wall conduction on B_3
Moisture transport	17	• Impermeable wall on B_1, B_2, and B_4 Symmetry on B_3	• Impermeable wall on all boundaries • Moderate Bi_m on B_4

$$\frac{\partial^2\psi}{\partial\eta\,\partial\xi}=0 \quad (20)$$

which enforces both:

$$\frac{\partial v_\xi}{\partial\xi}=0 \quad (21)$$

$$\frac{\partial v_\eta}{\partial\eta}=0 \quad (22)$$

This condition requires that the velocity is not changing at the free surface. It is necessary for the common situation of a headspace above the porous medium. With constant stream function specified on the other three boundaries, this gives the four conditions that are required mathematically and satisfies the physical condition of no flow through the walls or across the line of symmetry. The

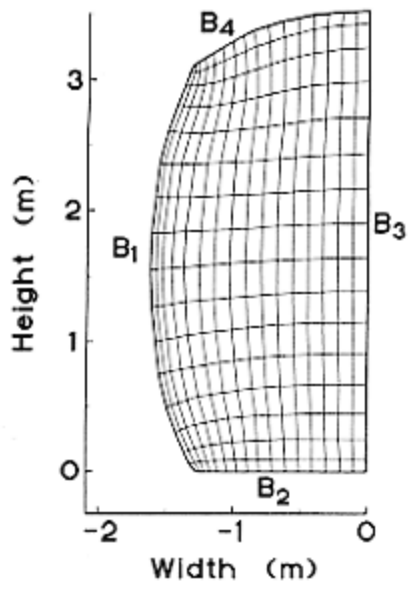

Figure 1–Finite difference mesh generated for model testing.

specification of a constant ($\psi = 0$) at the boundary was unchanged in the transformed plane. Equation 20 is written explicitly in the transformed plane so no mapping is required.

Energy Equations

For the energy equations, equations 15 and 16, conduction through the wall with a convective heat transfer coefficient on the outside of the wall, yielding a moderate Biot number, is specified on the bottom, top, and left side boundaries, and symmetry on the right side boundary as standard boundary conditions. The case of moderate Biot number ($0.1 < Bi < 50$) was of interest because the resistance of the container walls combined with the resistance due to convection at the walls may result in Biot numbers in this range. The common condition of large Biot number ($Bi \geq 50$) is implicitly handled in the model as a special case. These standard boundary conditions were developed using a finite-volume method where each node is associated with its discreet volume and flows across all boundaries are equated to storage as shown in Appendix B. A sinusoidal varying ambient temperature was specified outside the walls.

The varying air velocities and temperature gradients yielded Biot numbers between 10 and 60 in the standard test simulation. The top and bottom boundary conditions may differ depending on the specific model applications. For example, when the flow boundary condition allowed fluid flow through the top boundary, convective heat transfer was used as an alternative boundary condition on the top surface. Some applications may also not allow the use of a symmetry condition, requiring a wall condition on that side boundary also. Another alternative energy boundary condition is the basic condition of a single initial step change in the temperature on all boundaries. This step change boundary condition was also investigated in preliminary studies.

Moisture Transport Equation

For moisture transport, equation 17, no diffusion was specified through the bottom, top, and left side walls, and across the right hand line of symmetry. These standard boundary conditions were also developed using the finite-volume method. The top boundary condition and symmetry condition on this equation may also be expected to vary, depending on the application. As with the energy equations, when the flow boundary condition allowed fluid flow through the top boundary, convective mass transfer was used as the boundary condition on the top surface. The finite-volume development of these boundary conditions was similar to the example in Appendix B.

Initial Conditions

The primary initial condition was the initial temperature of the solid particles. This was generally chosen to be a relatively low temperature typical of products from refrigerated storage, since this gave large gradients and constituted the most difficult case for the model. Interstitial air was initially set in temperature and moisture equilibrium with the solid particles. Air velocities in the pore spaces were initialized as zero; however, the initial velocities had little effect on the simulations.

Since time was not changed in the transformation (eq. 15c), no mapping of the initial condition was required. All boundary conditions for the energy and moisture transport equations were either constants or were explicitly developed in the transformed plane so that no further mapping was required.

Finite Difference Solution

Equations 14, 15, 16, and 17 were discretized with second order accurate central differences. Throughout the development, solution techniques and coding methods were selected to minimize computation time, without compromising accuracy, so the model would run efficiently on a personal computer. The solution technique for the majority of simulations was:

1. Solve the two energy equations simultaneously for the peanut and air temperatures at each node for the next time step using the modified Crank-Nicolson scheme (Crank and Nicolson, 1947), described below, with successive over-relaxation (SOR) (Anderson et al., 1984).
2. Solve the flow equation, equation 14, for the stream function at each interior node for the current time step using point Gauss-Seidel iteration (Anderson et al., 1984) with SOR.
3. Calculate the velocity components from the stream function using finite difference approximations to the derivatives in the definition of stream function.
4. Solve the moisture transport equation for the humidity ratio at each node for the current time step using modified Crank-Nicolson with SOR, and simultaneously calculate the peanut moisture content at each node using equation 12.
5. Update the boundary conditions.
6. Return to step 1 if desired total time has not been reached.

When a boundary condition of step change in temperature was used with the single energy equation model, both the energy and moisture transport equations were solved explicitly. In that case, steps 1 and 4 were different in that temperature and humidity ratio, respectively, were calculated at each node using the simple explicit method (Anderson et al., 1984). The explicit methods required prohibitively small time steps (for stability) when varying ambient temperature boundary conditions were used.

The finite difference solution technique given above was coded for use in conjunction with a mesh generation program based on the method of Thompson et al. (1977). The mesh generation program will generate a mesh to fit any two-dimensional body when the physical (real) x,y coordinates of the boundary nodes are specified. This program solves equations 18 and 19 for the coordinates of the transformed plane using point Gauss-Seidel iteration with SOR. A 17×17 node mesh generated for the geometry of a railcar is shown in figure 1. This mesh was used for the standard test simulation. The mesh was slightly modified by leaving an open headspace at the top when testing the alternative free surface boundary condition, equation 20. Mesh sizes ranging from 9×9 nodes to 33×33 nodes were tested for the symmetric railcar geometry to test the effect of mesh size on accuracy. The railcar was assumed to have shelled peanuts as the

porous medium. Properties for the peanuts were taken from Steele (1974) and Suter et al. (1975). The values of h_l were taken as that for airflow over spheres using the air velocities in the pore space calculated by the model. The finite difference model was then used to predict the local temperatures, bulk air velocities, air moisture content, and peanut moisture content, as a function of time for the specified boundary conditions within the body described by the geometry of the meshes.

The computer model was also used to simulate conditions in a hypothetical railcar that was subject to relatively severe conditions, this will be referred to as the standard test simulation. This hypothetical railcar was loaded with shelled peanuts from refrigerated storage, at 4° C, and then subjected to a daily average maximum ambient temperature of 38° C and minimum of 21° C for the entire shipment time. Different conditions typical of storage and transportation situations were simulated, but the severe conditions of the standard test simulation was the most difficult case found for the model because of the large and varying gradients that resulted.

There are basically two temperature boundary conditions possible for these storage and transportation problems. A simple step change could be employed by using the average daily temperature. A more realistic boundary condition is to use the actual diurnally varying ambient temperature. This results in relatively large gradients to be imposed on the temperature field every day as the temperature cycles between the daily maximum and minimum. The constant imposing of large gradients is more difficult for numerical models than the step change condition. Thus, the most severe possible case is when the daily temperature variation is a maximum. This is the severe case chosen as the standard test simulation.

Results and Discussion

The alternative free surface boundary condition (eq. 20) worked well with the stream function solution. Figure 2 shows the predicted streamlines for the standard test in the rail car peanut bed after 24 h (at 12:00 noon), which was approximately the time of maximum velocities in the bed. An important measure of the effectiveness of the alternative flow boundary condition was its ability to enforce the conservation of mass at the top surface. Physically, all of the mass flow (of air) out through this boundary must reenter through another part of the boundary because the headspace is closed except for this boundary. No practical boundary condition was found that could explicitly enforce this conservation. The mass flows in and out of the headspace through the top surface of the peanuts are compared in figure 3 for the standard test simulation modified with this alternative condition, equation 20. After the first few hours the flow difference settled into a diurnal cycle that generally stayed within 10% of exact conservation of mass at the extremes of error.

Typical of porous media with stored agricultural products like grains and nuts, the one tested (shelled peanuts) offered a sufficiently high resistance to flow so that the air velocities from natural convection were quite low, as can be seen in the velocity profile in figure 4. This velocity profile is the y-component of velocity at the vertical midpoint. The maximum velocity achieved was

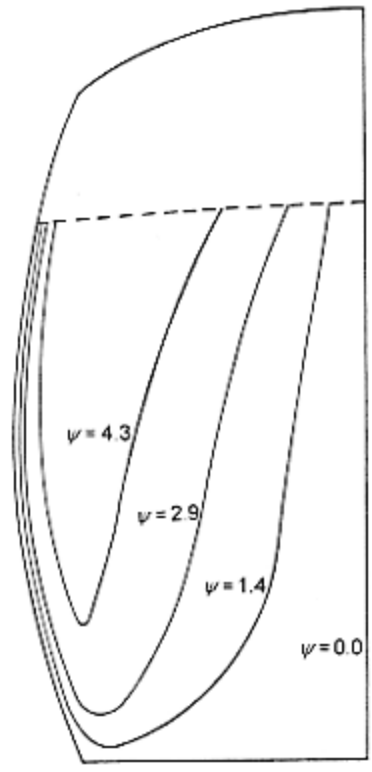

Figure 2–Streamlines in the porous medium after 24 h for an alternative test.

0.05 cm/s. The low velocities generally had little effect on the temperature solution, with one exception near the wall at the top surface of the bed. This was the point of maximum velocities and there was as much as 4° C difference between the model's prediction with and without convection included. The airflow lowered temperatures at this location during the day as relatively cool air from within the bed flowed up to the top surface.

The model was used to solve the governing equations with the mesh generated for the railcar geometry. A modified Crank-Nicolson solution technique was developed for equations 15, 16, and 17 to avoid instability problems stemming from the source terms, especially in equations 16 and 17, the fluid energy equation and the moisture transport equation. An explicit solution was attempted, as well as an alternating direction implicit

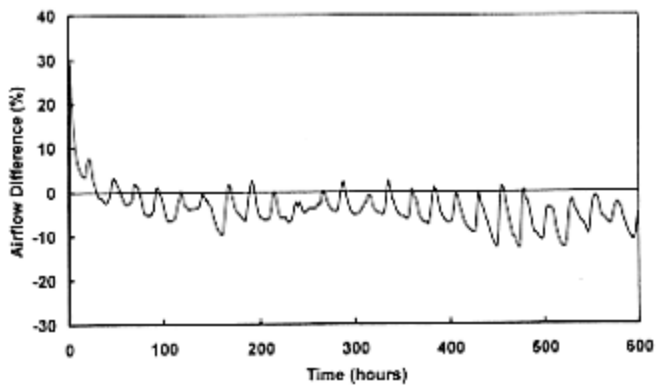

Figure 3–Mass balance at top surface of the peanuts, difference between flow in and out.

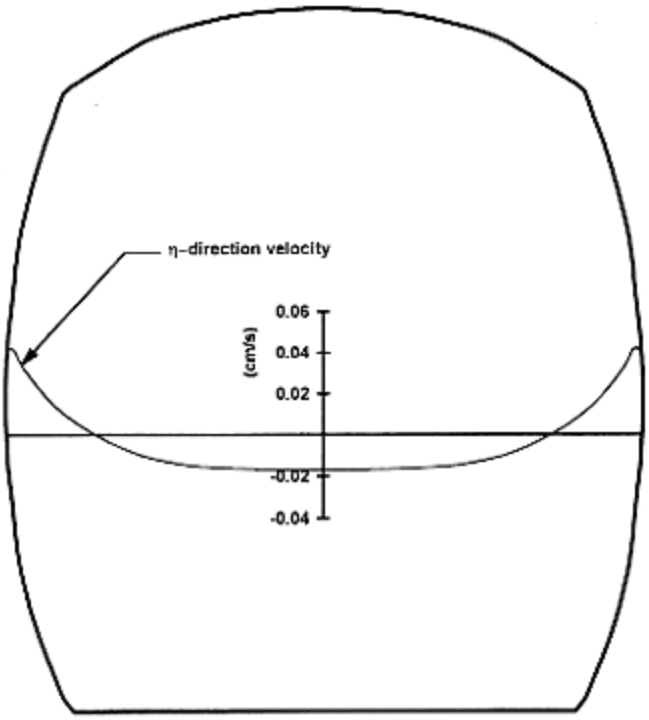

Figure 4–Velocity profile at the vertical midpoint.

(ADI) method, but neither of these worked as well with the diurnally varying temperature boundary condition. When a step change in temperature was used as a boundary condition, a simple explicit solution worked well. The standard method (Crank-Nicolson, 1947) is essentially an arithmetic average of the fully explicit and fully implicit methods. Fifty percent of each term is carried at the current time step and fifty percent is lagged at the previous time step. While this method is unconditionally stable for many cases, it was not unconditionally stable when used with equations 15, 16, and 17 because of the source terms in those equations. In equations 16 and 17 the source terms often dominated the equations when there was rapid heat and moisture transfer, respectively. This rapid heat and moisture transfer occurred twice a day when the diurnally varying temperature boundary condition was used. With the modified Crank-Nicolson solution the entire source term, e.g., $St_f(\theta_f - \theta_s)$ in the fluid energy equation, was carried at the current time step, instead of lagging half at the previous time step, thus placing all of that large term on the main diagonal of the solution matrix and insuring diagonal dominance of the matrix. The modified Crank-Nicolson method was stable with a time step twice as large as could be used with the standard Crank-Nicolson method.

Because of the convective terms and the source terms in the equations, the Crank-Nicolson method was not unconditionally stable, but the modified technique worked well and was stable with the energy equations for time steps of 60 min and a maximum modified Rayleigh number of 185. The solution of the moisture transport equation was stable for time steps up to 15 to 30 min. A 15-min time step gave stable solutions for all of the conditions that were tested, and this was the time step used with all model equations for calculations in the standard test simulation. Other time steps were only used to test the accuracy and stability of the model. Time steps less than 15 min did not affect the solutions, which shows that the 15-min time step gave sufficient accuracy. The 30-min time step generally gave stable solutions for less severe conditions, but occasionally produced instability at the top boundary during times of rapid moisture transfer. In these cases, reducing the time step to 15 min solved the instability problems. Both the energy and moisture equations had greater stability problems at the initial time steps because of the large step change in the boundary conditions initially combined with the ever present source terms, so smaller time steps were used for the first 1 to 3 h of simulation, starting at 1% of the base time step size and increasing in two-step changes to the base time step after the first 1 to 3 h of simulation.

An SOR parameter of 1.4 was effective in speeding up the convergence of the energy equation, except at the boundary nodes that were being calculated as part of the solution after using the control volume formulation. At these boundary nodes an under-relaxation parameter was used to insure stability. A value of 0.8 was sufficient with the one-half hour time steps, and a value of 1.0 worked for time steps of 0.1 h, and less. For the moisture transport equation, an SOR parameter of 1.2 worked best for the interior nodes with a value of 1.0 at the side boundary nodes. An under-relaxation parameter of 0.9 was required to insure stability at the top boundary nodes. After testing grids up to 33 × 33, we found no significant effect from grid refinements greater than 17 × 17.

A major difficulty during the model development was maintaining conservation of moisture in the porous medium. Figure 5 shows the change in total moisture in the porous medium predicted by the model for the standard test and indicates that a good overall moisture balance was obtained with the model. The most important factor that allowed the good moisture balances was insuring that the metrics from the mesh generation program were calculated with the same order finite difference equations as were the terms in the moisture transport equation. The finite-volume boundary conditions inherently gave first-order accurate differences; when a mesh generated with second-order accurate differences at the walls was used with these boundary conditions moisture was not conserved, which resulted in excessive drying of the particles at the boundaries.

A number of other possible causes of moisture loss were investigated but did not impact the moisture balance significantly. Some of the important possibilities are

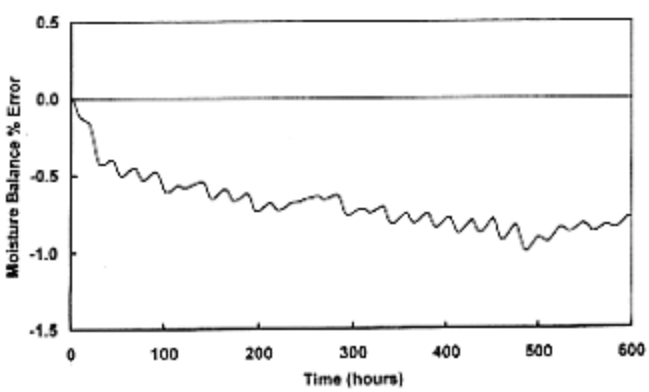

Figure 5–Predicted total moisture balance during the standard test.

discussed here. The solution of the moisture transport equation combined with the thin-layer drying equation for the particles may cause difficulty with maintaining a proper moisture balance between the air and the particles. Depending on the order of estimation, the successive estimation of air humidity ratio, particle moisture content, and equilibrium surface condition of the particle resulted in either an explicit moisture balance error or use of physically unrealistic driving gradients. This problem was circumvented by simultaneous estimation of the three variables using an iterative procedure. The simultaneous solution procedure caused the model to run slightly slower, but made little improvement in the moisture balance. It was expected that using boundary conditions developed by the finite volume method along with equation 17, developed by transformation, could prevent conservation of moisture because the two methods of development did not result in identical equations. However, simulation results showed little difference between the equations and the moisture balance problems persisted. Computer round-off and accuracy issues were also investigated and found not to be a problem. Hence the moisture balance problem was primarily attributed to improper differencing of the metrics.

The energy model (two energy equations, eqs. 15 and 16) was compared to an analytical solution of heat transfer in a semi-infinite solid with a sinusoidally varying surface temperature described by:

$$\theta(0,t) = A \sin(\omega t - \varepsilon_b) + \theta_{sa} \qquad (23)$$

For short times, the nodes near the surface of the porous medium may be considered as in a semi-infinite medium. Carslaw and Jaeger (1959) gave the analytical solution of this semi-infinite medium problem as:

$$\theta(x,t) = \frac{2A}{\sqrt{\pi}} \int_{\frac{x}{2\sqrt{\alpha_t t}}}^{\infty} \left(\sin\left[\omega \left(t - \frac{x^2}{4\alpha_t \mu^2} \right) - \varepsilon_b \right] + \theta_{sa} \right) e^{-\mu^2} d\mu \qquad (24)$$

For these tests the model was modified (by eliminating moisture transfer, airflow, and the thermal resistance of the container wall) to match this analytical solution. The standard time step of 15 min was used in the simulation.

Figure 6 shows that the model results compare well with the corresponding analytical solution. The worst case was the node nearest to the surface (0.029 m from the surface), which resulted in a 0.35° C standard error of difference for the first 96 h of simulation. This demonstrated that the two energy equation models for heat transfer, equations 15 and 16, effectively described the overall heat transfer in the porous medium.

The two-energy equation model indicated differences between the solid and fluid temperatures in the porous medium. The differences were largest near the side boundaries, during the high midday heating periods, and at the top surface when high temperatures due to solar heating were assumed. The temperature difference at the top of the porous medium was as large as 0.5° C at midday during the standard test. These temperature differences contribute to driving more moisture from the solid particles during the day, which gave a greater potential for moisture condensation at night. Future research is needed to confirm this temperature difference.

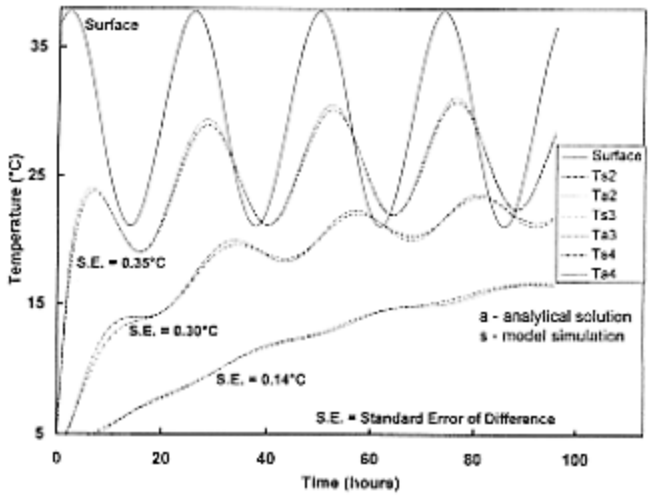

Figure 6–Comparison of heat transfer to analytical solution for three nodes nearest boundary.

CONCLUSIONS

A finite difference model was developed to simulate heat and moisture transfer in arbitrarily shaped porous media due to diffusion and convection. The model required 0.4 h of CPU time per day of simulation on a 386-33 MHz personal computer. The following conclusions were formulated from the results of this study:

- The instabilities from the source terms combined with diurnally varying boundary conditions with the energy and moisture transport equations were controlled by using a modified Crank-Nicolson method with the source term at the current time step, under-relaxing at the boundaries, and using small initial time step sizes.
- The two-energy equation model effectively described the overall heat transfer in the porous medium.
- The two-energy equation model predicts temperature differences as large as 0.5° C between the air and solid particles particularly near the boundaries with diurnally varying temperatures using the current estimates of thermal properties.
- The natural convection currents contribute significantly to the temperature solution at the upper corners of the porous medium.
- The free surface boundary condition, equation 20, gave a stable solution of the stream function equation and physically reasonable airflows through the boundary into the headspace.
- The finite difference model developed will predict the moisture migration due to short-term and long-term effects during storage and shipment of hygroscopic materials in containers that may be

described by arbitrarily shaped two-dimensional geometries.

ACKNOWLEDGMENT. The authors thank The Procter & Gamble Company, Cincinnati, Ohio, for providing part of the funds, equipment, and personnel for this research.

REFERENCES

Abbouda, S. K, P. A. Seib, D. S. Chung and A. Song. 1992. Heat and mass transfer in stored milo. Part II. Mass transfer model. *Transactions of the ASAE* 35(5):1575-1580.

Anderson, D. A., J. C. Tannehill and R. H. Pletcher. 1984. *Computational Fluid Mechanics and Heat Transfer*, 130-135. New York: Hemisphere.

ASAE Standards, 38th Ed. 1991. D245.4. Moisture relationships of grains, 363-367. St. Joseph, Mich.: ASAE.

Bear, J. 1972. *Dynamics of Fluid in Porous Media*, 738. New York: American Elsevier.

Carslaw, H. S. and J. C. Jaeger. 1959. *Conduction of Heat in Solids*, 2nd Ed. London: Oxford University Press.

Casada, M. E. 1990. Simulation of heat transfer and moisture migration during transportation of shelled peanuts. Unpub. Ph.D. thesis, North Carolina State University, Raleigh.

Casada, M. E. and J. H. Young. 1994. Heat and moisture transfer during transportation of shelled peanuts. *Transactions of the ASAE* 37(6):1939-1946.

Combarnous, M. A. and S. A. Bories. 1974. Modelisation de la coisation de la convection naturelle au sein d'une couche poreuse horizontale a l'aide d'un coefficient de transfert solide-fluide. *Int. J. of Heat and Mass Transfer* 17(14):505-515.

————. 1975. Hydrothermal convection in saturated porous media. In *Advances in Hydrosci.*, ed. V. T. Chow. 10:231-307.

Crank, J. and P. Nicolson. 1947. A practical method for numerical evaluation of solutions of partial differential equations of the heat-conduction type. In *Proc. of the Cambridge Philos. Society* 43:50-67.

Darcy, H. 1856. *Les Fontaines Publiques de la Ville de Dijon*. Paris: Dalmont. [As cited in Bear (1972)].

El-Khatib, G. and V. Prasad. 1987. Effects of stratification on thermal convection in horizontal porous layers with localized heating from below. *ASME J. of Heat Transfer* 109(3):683-687.

Ergun, S. 1952. Fluid flow through packed columns. *Chemical Eng. Progress* 48(2):89-94.

Halderson, J. L., J. E. Dixon and J. B. Johnson. 1991. Maintaining stored grain quality. CIS No. 518. College of Agriculture, Univ. of Idaho, Moscow.

Israeli, M. 1970. A fast implicit numerical method for time dependent viscous flows. *Studies in Applied Mathematics* 49(4):327-349.

Jayas, D. S., K. Alagusundaram, G. Shunmugam, W. E. Muir and N. D. G. White. 1992. Simulations of temperatures in stored bulks of wheat using a three-dimensional finite element model. ASAE Paper No. 92-6527. St. Joseph, Mich.: ASAE.

Kays, W. M. and M. E. Crawford. 1980. *Convective Heat and Mass Transfer*, 2nd Ed. New York: McGraw-Hill.

Khankari, K. K., R. V. Morey and S. V. Patankar. 1990. Moisture diffusion in stored grain due to temperature gradients. ASAE Paper No. 90-6581. St. Joseph, Mich.: ASAE.

————. 1993a. Application of a numerical model for prediction of moisture migration in stored grain. ASAE Paper No. 93-6018. St. Joseph, Mich.: ASAE.

Khankari K. K., S. V. Patankar and R. V. Morey. 1993b. A mathematical model for natural convection moisture migration in stored grain. ASAE Paper No.93-6017. St Joseph, Mich.: ASAE.

Loewer, O. J., I. J. Ross and G. M. White. 1979. Aeration, inspection and sampling of grain in storage bins. Cooperative Extension Publication AEN-45. Lexington: Univ. of Kentucky.

Masamune, S. and J. M. Smith. 1963. Thermal conductivity of beds of spherical particles. *I&EC Fundamentals* 2(2):136-143.

Muir, W. E. 1973. Temperature and moisture in grain storages. In *Grain Storage: Part of a System*, eds. R. N. Sinha and W. E. Muir, 49-69. Westport, Conn.: AVI.

Nguyen, T. V. 1986. Modeling temperature and moisture changes resulting from natural convection in grain storages. In *Preserving Grain Quality by Aeration and In-Store Drying*, eds. B. R. Champ and E. H. Highely, 81-87. ACIAR Proc. No. 15. Canberra, Australia: Australian Center for International Agricultural Research.

Obaldo, L. G., J. P. Harner and H. H. Converse. 1991. Prediction of moisture changes in stored corn. *Transactions of the ASAE* 34(4):1850-1858

Patterson, R. J., F. W. Bakker-Arkema and W. G. Bickert. 1971. Static pressure-airflow relationships in packed beds of granular biological materials such as grain – II. *Transactions of the ASAE* 17(1):172-174, 178.

Peyret, R. and T. D. Taylor. 1983. *Computational Methods for Fluid Flows*, 108-112. New York: Springer-Verlag.

Pierce, R. O. and D. P. Shelton. 1984. Aeration of stored grain. NebGuide G84-692. Lincoln: Cooperative Extension Service, Univ. of Nebraska.

Plumb, O. A. and L. A. Kennedy. 1977. Application of a k-ε turbulence model to natural convection from a vertical isothermal surface. *ASME J. of Heat Transfer* 99(1):79-85.

Prasad, V. 1987. Thermal convection in a rectangular cavity filled with a heat-generating, Darcy porous medium. *ASME J. of Heat Transfer* 109(3):697-703.

Prasad, V. and F. A. Kulacki. 1984a. Natural convection in a rectangular porous cavity with constant heat flux on one vertical wall. *ASME J. of Heat Transfer* 106(1):152-157.

Prasad, V. and F. A. Kulacki. 1984b. Convective heat transfer in a rectangular porous cavity – Effect of aspect ratio on flow structure and heat transfer. *ASME J. of Heat Transfer* 106(1):158-165.

————. 1986. Effects of the size of heat source on natural convection in horizontal porous layers heated from below. In *Proc. 8th Int. Heat Transfer Conf.* 5:2677-2682, San Francisco, Calif. New York: Hemisphere.

————. 1987. Natural convection in horizontal porous layers with localized heating from below. *ASME J. of Heat Transfer* 109(3):795-798.

Roache, P. J. 1972. *Computational Fluid Dynamics*, 139-146. Albuquerque, New Mexico: Hermosa.

Ross, L. J., H. E. Hamilton and G. M. White. 1973. Principles of grain storage. Cooperative Extension Publication AEN-20. Lexington: Univ. of Kentucky.

Sherwood, T. K. 1936. The air drying of solids. *Trans. Am. Inst. Chem. Eng.* 32(2):150-168.

Singh, A. K., E. Leonardi and G. R. Thorpe. 1993. *Transactions of the ASAE* 36(4):1159-1173.

Smith, J. S., Jr. and J. L Davidson, Jr. 1982. Psychrometrics and kernel moisture content u related to peanut storage. *Transactions of the ASAE* 25(1):231-236.

Steele, J. L. 1974. Resistance of peanuts to airflow. *Transactions of the ASAE* 17(3):573-577.

Stewart, W. E., Jr. and C. L. G. Dona. 1988. Free convection in a heat generating porous medium in a finite vertical cylinder. *ASME J. of Heat Transfer* 110(2):517-520.

Suter, D. A., K. K. Agrawal and B. L. Clary. 1975. Thermal properties of peanut pods, hulls and kernels. *Transactions of the ASAE* 18(2):370-375.

Tanka, H. and K. Yoshida. 1984. Heat and mass transfer mechanisms in a grain storage silo. In *Engineering and Food*, ed. B. M. McKenna, 89-98; vol I. Engineering Sciences in the Food Industry. Essex, England: Elsevier Science Pubs.

Thames, F. C., J. F. Thompson and C. W. Mastin. 1975. Numerical solution of the Navier-Stokes equations for arbitrary two-dimensional airfoils. In *Proc. of NASA Conf. on Aerodynamic Analysis Requiring Advanced Computers*, 469-495. Langley Research Center. NASA SP-347.

Thompson, J. F. 1978. Numerical solution of flow problems using body-fitted coordinate systems. In *Computational Fluid Dynamics*, ed. W. Kollmann, 1-95. New York: Hemisphere.

Thompson, J. F., F. C. Thames and C. W. Mastin. 1974. Automatic numerical generation of boundary-fitted curvilinear coordinate system for field containing any number of arbitrary two-dimensional bodies. *J. of Computational Physics* 15(3):299-319.

———. 1977. *Boundary-fitted Curvilinear Coordinate System for Solution of Partial Differential Equations on Fields Containing any Number of Arbitrary Two-dimensional Bodies.* Langley Research Center. NASA CR-2729.

Touloukian, Y. S., P. E. Liley and S. C. Saxena. 1970a *Thermophysical Properties of Matter*, vol. 3: *Thermal Conductivity, Nonmetallic Gases and Liquids*. New York: IFI/Plenum.

Touloukian, Y. S. and T. Makita. 1970b. *Thermophysical Properties of Matter*, vol. 6: *Specific Heat, Nonmetallic Gases and Liquids*. New York: IFI/Plenum.

Touloukian, Y. S., S. C. Saxena and P. Hestermans. 1970c. *Thermophysical Properties of Matter*, vol. 11: Viscosity. New York: IFI/Plenum.

Vafai, K. and C. L. Tein. 1981. Boundary and inertia effects on flow and heat transfer in porous media. *Int. J. of Heat and Mass Transfer* 24(2):195-203.

Wakao, N. and S. Kaguei. 1982. *Heat and Mass Transfer in Packed Beds*, 264-295. New York: Gordon and Breach.

Wilcke, W. F. and L. D. Van Fossen. 1986. Managing corn in long term storage. Cooperative Extension Publication AE-3021. Ames: Iowa State University.

Wooding, R. A. 1957. Steady state free thermal convection of liquid in a saturated permeable medium. *J. of Fluid Mechanics* 2:273-285.

NOMENCLATURE

- c = specific heat (J/kg)
- g = acceleration due to gravity (m/s^2)
- h = node spacing (m)
- h^*_{fg} = latent heat of vaporization of water from solid particles (J/kg)
- h_m = convective mass transfer coefficient (m/s)
- h_p = convective heat transfer coefficient at peanut kernel surface (W/m^2K)
- $h_{w,i}$ = convective heat transfer coefficient on inside of container wall (W/m^2K)
- $h_{w,o}$ = convective heat transfer coefficient on outside of container wall (W/m^2K)
- k_e = effective thermal conductivity of porous medium (W/mK)
- $\bar{k}_f$ = equivalent thermal conductivity tensor in the fluid path (W/mK)
- $\bar{k}_s$ = equivalent thermal conductivity tensor in the solid matrix (W/mK)
- q = heat flux (W/m^2)
- t = time (s)
- $\bar{t}$ = t = (trivial) transformation of time (s)
- u = x-component of velocity (m/s)
- v = y-component of velocity (m/s)
- x,y = coordinates
- $A_{s/v}$ = surface area per unit volume of solid, l/m; [= $(6/D_p)(1-\phi)$ for spheres]
- D_m = $D'_m \rho_s \beta_m$ (m^2/s); (= Fick's Law mass diffusion coefficient for porous media)
- D'_m = modified mass diffusion coefficient for porous media (m^2/s)
- D_p = equivalent particle diameter (m)
- F_1 = Ergun's first coefficient, $Pa \cdot s/m^2$ ($kg/m^3 \cdot s$)
- F_2 = Ergun's second coefficient, $Pa \cdot s^2/m^3$ (kg/m^4)
- F^* = $F \phi g (\sqrt{K} / \mu)$ (s/m)
- K = permeability of porous medium (m^2)
- L = characteristic length, y-direction (m)
- M = dry basis moisture content (decimal)
- M_o = initial particle moisture content (decimal)
- M_w = rate of evaporation or condensation per unit volume ($kg/s \cdot m^3$)
- P = pressure (Pa)
- T = temperature (K)
- T_o = reference temperature for equation of state (K)
- V = Darcian velocity vector (m/s)
- V_b = apparent (bulk or Darcian) velocity (m/s)
- V_p = V_b/ϕ = pore velocity (m/s)
- V_ξ = v_ξ = velocity normal to lines of constant ξ (m/s)
- V_η = v_η = velocity normal to lines of constant η (m/s)

SUBSCRIPTS

- a = air; f = fluid; o = initial time; s = solid; t = total; w = wall

SUPERSCRIPTS

- n = last time step; $n+1$ = new time step

GREEK SYMBOLS

- α_e = coefficient of thermal expansion of air (l/K)
- α_f, α_f = fluid and solid phase thermal diffusitvity, respectively (m^2/s)
- β_m = slope of equilibrium moisture content isotherm for solid particles (m^3/kg)
- $\bar{\gamma}$ = humidity ratio ($kg_{H_2O}/kg_{dry\ air}$)
- ϵ_b = boundary temperature phase constant = 14 h
- μ = dynamic viscosity (Pa·s)
- ν = kinematic viscosity (m^2/s)
- ρ = density (kg/m^3)
- ρ_o = reference density of air in equation of state (kg/m^3)
- ρ_s = dry matter density of solid particulates (kg/m^3)
- ϕ = void fraction of porous medium = porosity (decimal)
- ω = boundary temperature oscillation frequency (Hz)

DIMENSIONLESS VARIABLES

- $\bar{x}$ = x/L
- $\bar{y}$ = y/L
- F = $F_2\sqrt{K} / (\rho \phi)$ = Forchheimer coefficient
- F_u = $1 + 2uF^*$
- F_v = $1 + 2vF^*$
- H_{fg} = $(h^*_{fg} M_o) / [C_s (T_w - T_o)]$
- J = $\bar{x}_\xi \bar{y}_\eta - \bar{y}_\xi \bar{x}_\eta$ = inverse of Jacobean of the transformation

H_w = $2 L^2 h_{w,i} / (\phi k_f)$ = dimensionless wall convective heat transfer coefficient
Le_f = D_m/α_f = fluid phase Lewis number
Ra^* = $(\rho g \alpha_e K L \Delta T) / (\mu \alpha_t)$ = Rayleigh number
Re_p = $D_p V_p g/\mu$ = particle Reynolds number
St_m = $[6h_m L^2(1-\phi)] / [D_p \alpha_t \phi]$ = modified moisture Stanton number
St_f = $[6h_p L^2(1-\phi)] / [D_p k_f \phi]$ = modified fluid Stanton number
St_s = $[6h_p L^2] / [D_p (\rho c)_s \alpha_f]$ = modified solid Stanton number
$V = \frac{L}{\phi\alpha_f} v$ = dimensionless velocity
$\alpha = \bar{x}_\eta^2 + \bar{y}_\eta^2$ (transformation metric)
$\beta = \bar{x}_\xi \bar{x}_\eta + \bar{y}_\xi \bar{y}_\eta$ (transformation metric)
$\gamma = \bar{x}_\xi^2 + \bar{y}_\xi^2$ (transformation metric)
$\delta = \alpha(\bar{y}_{\xi\xi}\bar{x}_\eta - \bar{x}_{\xi\xi}\bar{y}_\eta) - 2\beta(\bar{y}_{\xi\eta}\bar{x}_\xi - \bar{x}_{\xi\eta}\bar{y}_\xi) + \gamma(\bar{x}_{\eta\eta}\bar{y}_\xi - \bar{y}_{\eta\eta}\bar{x}_\xi)$ (transformation metric)
$\varepsilon = \alpha(\bar{x}_{\xi\xi}\bar{y}_\xi - \bar{y}_{\xi\xi}\bar{x}_\eta) - 2\beta(\bar{x}_{\xi\eta}\bar{y}_\eta - \bar{x}_{\xi\eta}\bar{y}_\eta) - \gamma(\bar{y}_{\eta\eta}\bar{x}_\eta - \bar{x}_{\eta\eta}\bar{y}_\eta)$ (transformation metric)
$\theta = (T - T_o)/(T_w - T_o)$
θ_{SA} = daily mean temperature
η = generalized coordinate
ξ = generalized coordinate
$\tau = (t\alpha_t)/D^2$ = dimensionless time
ψ = stream function
$\Gamma = \bar{\gamma}/\bar{\gamma}_o$
$\Omega = M/M_o$

APPENDIX A

RELATIONSHIPS IN THE TRANSFORMED PLANE

The following notation is used in this appendix:

$f(x,y,t)$ = a twice continuously differentiable scalar function of x, y, and t
t_ξ = unit vector tangent to a line of constant ξ
t_η = unit vector tangent to a line of constant η
f_ξ = $\partial f/\partial_\xi$ and $f\eta = \partial f/\partial\eta$

The normal and tangential derivatives in the transformed plane are given by Thompson (1978). Normal velocities are then:

$$\bar{V}_\eta = \frac{\partial\psi}{\partial t_\eta} = \frac{\partial\psi}{\partial\xi} / \sqrt{\gamma} = \frac{1}{\sqrt{\gamma}}\left(\frac{\partial\psi}{\partial\bar{x}} x_\xi + \frac{\partial\psi}{\partial\bar{y}} y_\xi\right) \quad (A1)$$

$$V_\eta = \frac{1}{\sqrt{\gamma}}\left(\frac{\phi\alpha_f}{L}\frac{\partial\psi}{\partial\bar{x}} x_\xi + \frac{\phi\alpha_f}{L}\frac{\partial\psi}{\partial\bar{y}} y_\xi\right) \quad (A2)$$

giving:

$$V_\eta = \frac{\phi\alpha_f}{L\sqrt{\gamma}}\frac{\partial\psi}{\partial\xi} \quad (A3)$$

and

$$\bar{V}_\xi = \frac{\partial\psi}{\partial t_\xi} = \frac{\partial\psi}{\partial\xi} / \sqrt{\alpha} = \frac{-1}{\sqrt{\alpha}}\left(\frac{\partial\psi}{\partial\bar{x}} x_\eta + \frac{\partial\psi}{\partial\bar{y}} y_\eta\right) \quad (A4)$$

$$V_\xi = \frac{-1}{\sqrt{\alpha}}\left(\frac{\phi\alpha_f}{L}\frac{\partial\psi}{\partial\bar{x}} x_\eta + \frac{\phi\alpha_f}{L}\frac{\partial\psi}{\partial\bar{y}} y_\eta\right) \quad (A5)$$

giving:

$$V_\xi = \frac{\phi\alpha_f}{L\sqrt{\alpha}}\frac{\partial\psi}{\partial\xi} \quad (A6)$$

APPENDIX B

IMPLEMENTATION OF BOUNDARY CONDITIONS

Because there is little information available in the literature on the finite-volume development of boundary conditions in the transformed plane, the development is demonstrated in this example. The condition on the fluid energy equation at the left side wall was developed from the finite-volume shown in figure B1. Using the relationships in Appendix A and in Thompson (1978), the heat fluxes normal to each surface are:

$$q_1 = -\frac{h\sqrt{\gamma}}{2} k_f \frac{1}{J\sqrt{\gamma}} \times\left\{\gamma\left[(T_f)_{1,j+1} - (T_f)_{1,j}\right] - \beta\left[(T_f)_{2,j} - (T_f)_{1,j}\right]\right\} + \frac{h\sqrt{\gamma}}{2} V_\eta \frac{1}{2}\left[(T_f)_{1,j} + (T_f)_{1,j+1}\right] \quad (B1)$$

$$q_2 = -h\sqrt{\alpha}\frac{k_f}{J\sqrt{\alpha}} \times\left\{\alpha\left[(T_f)_{2,j} - (T_f)_{1,j}\right] - \frac{\beta}{2}\left[(T_f)_{1,j+1} - (T_f)_{1,j+1}\right]\right\} + \frac{h\sqrt{\alpha}}{2} V_\xi \frac{1}{2}\left[(T_f)_{1,j} + (T_f)_{2,j}\right] \quad (B2)$$

$$q_3 = -\frac{h\sqrt{\gamma}}{2} k_f \frac{1}{J\sqrt{\gamma}} \times\left\{\gamma\left[(T_f)_{1,j} - (T_f)_{1,j-1}\right] - \beta\left[(T_f)_{2,j} - (T_f)_{1,j}\right]\right\} + \frac{h\sqrt{\gamma}}{2} V_\eta \frac{1}{2}\left[(T_f)_{1,j} + (T_f)_{1,j-1}\right] \quad (B3)$$

$$q_4 = h\sqrt{\alpha}\, h_{w,i}\left[T_{w,i} - (T_f)_{1,j}\right] \quad (B4)$$

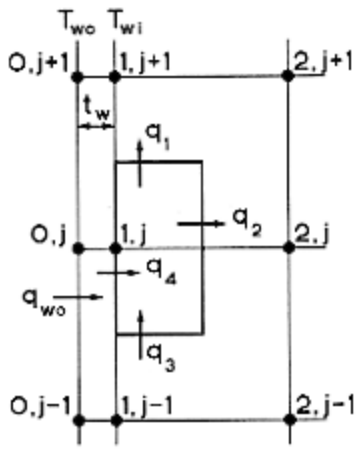

Figure B1–Energy balance at side wall of railcar.

When these fluxes are summed with the source term and set equal to energy storage, the result is:

$$\phi(\rho c_f)\frac{Jh^2}{2}\frac{\partial(T_f)_{1,j}}{\partial t} =$$

$$\frac{Jh^2}{2}h_p A_{s/v}\left[(T_s)_{1,j} - (T_f)_{1,j}\right] + q_1 - q_2 - q_3 + q_4 \quad \text{(B5)}$$

Substituting equations B1 through B4 into equation B5 and cancelling terms yield:

$$\frac{\partial(T_f)_{1,j}}{\partial t} = \frac{h_m A_{s/v}}{\phi}\left[(T_s)_{1,j} - (T_f)_{1,j}\right] + \frac{\alpha_f L}{J^2\phi}\left\{\alpha\left[(T_f)_{2,j} - (T_f)_{1,j}\right] - \frac{\beta}{2}\left[(T_f)_{1,j+1} - (T_f)_{1,j-1}\right] + \gamma\left[(T_f)_{1,j+1} - 2(T_f)_{1,j} + (T_f)_{1,j-1}\right]\right\} - \frac{V_\eta}{2J\phi}\left[(T_f)_{1,j+1} - (T_f)_{1,j-1}\right] - \frac{V_\xi}{2J\phi}\left[(T_f)_{1,j} + (T_f)_{2,j}\right] \quad \text{(B6)}$$

which, in dimensionless variables, becomes:

$$\frac{\partial(\theta_f)_{1,j}}{\partial\tau} = \mathfrak{B}_h\left[(\theta_s)_{1,j} - (\theta_f)_{1,j}\right] + H_w\frac{\sqrt{\alpha}}{J}\left[\theta_{w,i} - (\theta_f)_{1,j}\right] + \frac{L^2}{\phi J^2}\left\{2\alpha\left[(\theta_f)_{2,j} - (\theta_f)_{1,j}\right] - \beta\left[(\theta_f)_{1,j+1} - (\theta_f)_{1,j-1}\right] + \gamma\left[(\theta_f)_{1,j+1} - 2(\theta_f)_{1,j} + (\theta_f)_{1,j-1}\right]\right\} - \frac{L^2 V_\eta}{2J\phi\alpha_f}\left[(\theta_f)_{1,j+1} - (\theta_f)_{1,j-1}\right] - \frac{L^2 V_\xi}{2J\phi\alpha_f}\left\{\left[(\theta_f)_{1,j} + (\theta_f)_{2,j}\right] - \frac{T_o}{T_w - T_o}\right\} \quad \text{(B7)}$$